Technical University of Denmark

DTU

Saturation-recovery metabolicexchange rate imaging with hyperpolarized [113C] pyruvate using spectralspatial excitation

Schulte, Rolf F.; Sperl, Jonathan I.; Weidl, Eliane; Menzel, Marion I.; Janich, Martin A.; Khegai, Oleksandr; Durst, Markus; Ardenkjær-Larsen, Jan Henrik; Glaser, Steffen J.; Haase, Axel; Schwaiger, Markus; Wiesinger, Florian

DTU Library
Technical Information Center of Denmark

Saturation-Recovery Metabolic-Exchange Rate Imaging with Hyperpolarized [1-^{13}C]Pyruvate Using Spectral-Spatial Excitation

Rolf F. Schulte,[1]* Jonathan I. Sperl,[1] Eliane Weidl,[2] Marion I. Menzel,[1] Martin A. Janich,[1,2,3] Oleksandr Khegai,[1,2,3] Markus Durst,[1,5] Jan Henrik Ardenkjaer-Larsen,[4,6] Steffen J. Glaser,[3] Axel Haase,[5] Markus Schwaiger,[2] and Florian Wiesinger[1]

Within the last decade hyperpolarized [1-^{13}C]pyruvate chemical-shift imaging has demonstrated impressive potential for metabolic MR imaging for a wide range of applications in oncology, cardiology, and neurology. In this work, a highly efficient pulse sequence is described for time-resolved, multislice chemical shift imaging of the injected substrate and obtained downstream metabolites. Using spectral-spatial excitation in combination with single-shot spiral data acquisition, the overall encoding is evenly distributed between excitation and signal reception, allowing the encoding of one full two-dimensional metabolite image per excitation. The signal-to-noise ratio can be flexibly adjusted and optimized using lower flip angles for the pyruvate substrate and larger ones for the downstream metabolites. Selectively adjusting the excitation of the down-stream metabolites to 90° leads to a so-called "saturation-recovery" scheme with the detected signal content being determined by forward conversion of the available pyruvate. In case of repetitive excitations, the polarization is preserved using smaller flip angles for pyruvate. Metabolic exchange rates are determined spatially resolved from the metabolite images using a simplified two-site exchange model. This novel contrast is an important step toward more quantitative metabolic imaging. Goal of this work was to derive, analyze, and implement this "saturation-recovery metabolic exchange rate imaging" and demonstrate its capabilities in four rats bearing subcutaneous tumors. **Magn Reson Med 69:1209–1216, 2013. © 2012 Wiley Periodicals, Inc.**

Key words: metabolic imaging; hyperpolarization; [1-^{13}C]pyruvate; saturation-recovery; metabolic exchange rate; magnetic resonance spectroscopy; spectral-spatial excitation

INTRODUCTION

Metabolic imaging with hyperpolarized substances is an emerging field to detect cellular metabolism minimally invasive (1–4). It involves labeling small endogenous molecules selectively with the stable ^{13}C isotope and polarizing these ^{13}C spins to very high levels via dynamic nuclear polarization. The samples are then rapidly dissolved to obtain injectable solutions (2). For metabolic imaging in vivo, target molecules generally must have long T_1 relaxation times and rapid metabolic turnover rates. The most-researched molecule currently is [1-^{13}C]pyruvate (Pyr), which has a $T_1 \approx 60$ s in vitro and a very fast conversion into [1-^{13}C]lactate (Lac), [1-^{13}C]alanine (Ala), and bicarbonate H^{13}CO$_3^-$ (BC), which can all be detected via magnetic resonance spectroscopy.

Pyr is an endogenous substance, which can be administered in fairly large doses. It is injected into a suitable vein and then transported through the blood stream to the region of interest like for instance a specific organ or a tumor. Pyr is rapidly taken up into the cells and converted enzymatically into Lac and Ala via lactate dehydrogenase and alanine transaminase, respectively. Although these are reversible reactions, the back-reactions are typically an order of magnitude lower and can be neglected for the short time duration of hyperpolarized experiments (5,6). Pyr also gets converted unidirectionally into acetyl-CoA via pyruvate dehydrogenase with the MR-visible ^{13}C label going to ^{13}CO$_2$, which is in rapid exchange with BC via carbonic anhydrase. BC can be detected in organs with high pyruvate dehydrogenase activity like the heart. In summary, Pyr and conversion to downstream metabolites can give valuable insights into the fundamental energy metabolism and has therefore high potential for diagnostic imaging in disorders with altered metabolism, such as cancer or stroke.

The challenge from an MR point of view is to encode multiple dimensions with a sufficiently high resolution in a short period of time: three spatial, one spectroscopic, and one temporal dimension. Spatial encoding of ideally three dimensions is generally desired to localize the region of interest. The spectroscopic dimension is required for being able to individually detect the injected molecule and its downstream metabolites. The kinetic dynamics are characterized by the bolus arrival of the injected compound and a subsequent conversion. To quantify the kinetics, acquisition of several time steps of this characteristic curve is desirable. Main boundary constraint of hyperpolarized MR is that the polarization disappears irrecoverably with T_1 relaxation and excitation into the transverse plane.

Various different encoding approaches have been investigated, which can be roughly divided into pulse-and-acquire type of sequences (7–16) and sequences using a refocusing of spins (spin-echo or steady-state free precession) (17,18). The most basic sequence is chemical shift imaging (CSI) with a small tip-angle excitation, which allows full spectral sampling with a low spatial resolution by sequential phase encoding (19). A faster encoding can be achieved with echo-planar spectroscopic imaging, where an alternating readout gradient encodes one spatial and the spectral dimension per excitation, hence superseding one-phase-encoding direction (20). Related but even more encoding efficient is a method called fast spiral CSI, where the small-tip angle excitation is followed by multiple spiral interleaves encoding two spatial and the spectral dimension (7,9,12). Higher spatial resolution can be achieved by spatial interleaving. Another way of encoding is called IDEAL Spiral CSI, where the excitation is followed by a single-shot spiral readout trajectory. The spectroscopic dimension is encoded by delaying the start of the spiral gradient waveform in the separate excitations (14). Many of the preceding methods sample the spectroscopic dimension sparsely and use the gained time to sample with higher spatial resolution and/or to acquire data at multiple time steps during metabolic conversion.

A different approach is to separate the spectral encoding from the acquisition by selectively exciting a single resonance with a spectral-spatial (SPSP) excitation pulse (21) and combine this with a pure imaging readout such as echo-planar imaging or single-shot spiral (22–26). SPSP pulses are two-dimensional (2D) pulses, combining frequency and slice-selective excitation into a single, fairly long radiofrequency pulse. By shifting the excitation frequency, it is possible to consecutively encode the different metabolites.

Acquiring multiple time steps in the metabolism is desired for quantifying the underlying kinetic processes. Following the injection of Pyr, it is possible to observe the Pyr bolus and its conversion into Lac, Ala, and BC. The signal curves start with a rapid increase followed by a smooth decay. The signal plateau is usually short. When acquiring metabolic images of only a single-time step, the signal level therefore highly depends on timing, perfusion, and conversion rates. The most common approach for acquiring multiple time steps is simple spectroscopy without spatial encoding. The region of interest is roughly selected by slice selection or a surface coil, and fully sampled spectra can be acquired with high temporal resolution. These kinetic curves can be used for metabolic modeling (6,27,28). More involved than pure spectral acquisition is to acquire time steps with some spatial encoding. With sufficient spatial and temporal resolution, it is possible to fit conversion rates on a pixel-by-pixel basis, hence acquiring metabolic-exchange rate images (29).

Saturating metabolites can be used to gain further information about the metabolism. In Ref. 30, the authors use a saturation and inversion of the pyruvate and lactate magnetization to proof that it is indeed an exchange reaction and to cross-validate fitting with a two-site exchange model. In Ref. 31, the authors saturate Lac with a frequency specific pulse and acquire metabolite images after a delay time of 4.55 s with a Spiral CSI encoding with three spatial interleaves with flip angles of 35.5°, 45°, and 90°, thereby finally

saturating all metabolites including Pyr. Hence, all magnetization in the next acquisition stems from inflowing polarized substrate. Metabolic modeling using Michaelis–Menten was performed on a region of interest. In both Refs. 30 and 31, the authors are not mapping metabolic exchange rates spatially localized.

The objective of this work is to acquire metabolic-exchange rate images in a simple manner without the need for intricated metabolic modeling methods. SPSP pulses are used to excite and at the same time, saturate downstream metabolites with 90°, leading to a recovery of magnetization for the next repetition by conversion. The precursor Pyr is excited with a small flip angle SPSP pulse to conserve polarization. SPSP pulses suitable for all resonances of the spectrum were designed by a direct 2D linear least-squares optimization. These pulses were implemented into a pulse-and-acquire sequence with a spiral readout. Both frequencies and flip angles of the SPSP pulses can be individually tailored to the desired application. Furthermore, signal-to-noise (SNR) simulations give insights into the optimal selection of flip angle and metabolite repetition time. Combining SPSP excitation and spiral readout allowed to detect quantitative metabolic exchange rates spatially localized. This novel contrast is an important step toward more quantitative metabolic imaging and has not been demonstrated before. The effectiveness of the approach is demonstrated by imaging four tumor-bearing rats. The concept was introduced with preliminary results initially on the ISMRM 2010 (24).

THEORY AND METHODS

Saturation Recovery

The metabolic conversion of Pyr into Lac, Ala or BC can be modeled by a simplified two-site exchange model (27,29,32)

$$\frac{dM_X}{dt} = k_{PX}M_P - \frac{1}{T_{1,X,eff}}M_X, \qquad [1]$$

where M_X and M_P denote the magnetization of downstream metabolite X (i.e., Lac, Ala, or BC) and Pyr, respectively. The conversion rate from Pyr to X is denoted by k_{PX}, whereas the loss of magnetization of X is given by an effective decay $T_{1,X,eff}$ composed of excitation, T_1 relaxation, back-conversion, and other smaller effects like in- and outflow differences. A typical curve, as shown in Fig. 1, is characterized by a Pyr bolus arrival, followed by rapid conversion into downstream metabolites X and a signal decay due to T_1 relaxation. Although the conversion rate remains approximately constant throughout the whole experiment, the relaxation term in Eq. [1] is small at the beginning of the conversion due to high Pyr signal level M_P and small downstream signal level M_X. The $M_X/T_{1,X,eff}$ term can therefore be neglected for sufficiently short times between repetitive excitations of the same metabolite. Including this assumption into Eq. [1] leads to

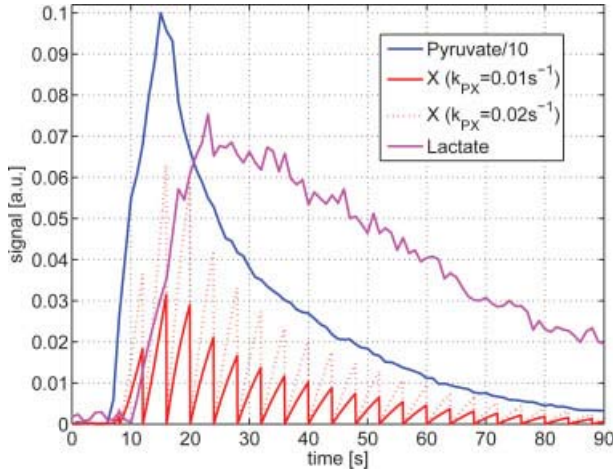$$k_{PX} = \frac{\Delta M_X}{\Delta t} \cdot \frac{1}{M_P}. \qquad [2]$$

FIG. 1. Signal evolution for the saturation-recovery experiment. The measured typical Pyr curve is shown in blue (scaled down by a factor of 10), whereas the measured Lac curve is shown in magenta. The saturation-recovery effect is simulated with the two-site exchange model (Eq. [1]) for typical values of $T_1 = 20\,$s, $t_m = 4\,$s and $k_{PX} = 0.01\,$s^{-1} (red solid), and $k_{PX} = 0.02\,$s^{-1} (red dotted). [Color figure can be viewed in the online issue, which is available at wileyonlinelibrary.com.]

When exciting Pyr with a sufficiently small flip angle θ_P and X with $\theta_X = 90°$, it is possible to excite X with good SNR, while at the same time, selectively saturating the existing magnetization of X. The signal acquired in the next excitation of X therefore stems from a recovery of magnetization M_X due to fresh conversion from the Pyr signal M_P. Because of this underlying principle, the method is called "saturation-recovery metabolic-exchange rate imaging". The sequence can be continuously repeated and the most suitable time step in terms of SNR and artifacts is chosen afterward.

With the detected signal (image intensity) given by $S = M \cdot \sin \theta$ and the selected $\theta_X = 90°$, Eq. [2] translates to

$$k_{PX} = \frac{S_X \cdot \sin \theta_P}{t_m \cdot (S_P + \alpha)}, \qquad [3]$$

where α denotes a regularization parameter to avoid division by zero or very small values of S_P. The time between repetitive excitations of the same metabolite is denoted by t_m and equivalent to pulse repetition time multiplied with the number of imaged metabolites. This equation allows to directly map the metabolic exchange rates of Pyr into its downstream metabolites if the SNR is sufficient and the relaxation term neglected. The effect of this simplification was estimated using Eq. [1], the Pyr curve in Fig. 1, and typical values of $k_{PX} = 0.01\,$s^{-1} or $0.02\,$s^{-1}, $T_{1,X,\mathrm{eff}} = 20\,$s and $t_m = 4\,$s. In this estimation, the error of the signal M_X due to omitting the $M_X/T_{1,X,\mathrm{eff}}$ term was $\lesssim 10\%$ in both cases of k_{PX}.

Spectral-Spatial Pulse Design

A general-purpose SPSP pulse was designed for metabolic imaging of Pyr and its downstream metabolites. That is, the spectral profile is suitable for exiting a single resonance of any of the present metabolites with minimal contamination

from the other resonances. The pulse was designed directly in two dimensions under the small-tip-angle approximation by a linear least-squares fit. The excitation matrix A has the entries

$$A_{m,n} = \exp(-2\pi\mathrm{i}(f_{1,m}k_{1,n} + f_{2,m}k_{2,n})), \qquad [4]$$

where $f_{1,m}$ and $f_{2,m}$ denote the discrete spatial and spectral frequencies, respectively. The spatial k-space locations $k_{1,n}$ are the integral over the zig-zag gradient modulation, which is determined by the maximum gradient strength, slew rate, and timings. The spectral k-space locations for a pulse of duration T is given by $k_{2,n} = T - t$. The desired excitation profile is given by

$$b_m = \begin{cases} 1 & \text{for } |f_{1,m}| < f_{P1} \text{ and } |f_{2,m}| < f_{P2} \\ 0 & \text{for } |f_{1,m}| > f_{S1} \text{ or } |f_{2,m}| > f_{S2}, \end{cases} \qquad [5]$$

with the pass- and stop-band frequencies being defined by $f_P = \frac{1}{2}\mathrm{BW}(1 - \mathrm{FTW})$ and $f_S = \frac{1}{2}\mathrm{BW}(1 + FTW)$, respectively. BW is the bandwidth and FTW is the fractional transition width. The transition band between f_P and f_S is undefined and no sampling points are included in this band for the fit. This profile is shifted in the spectral dimension to the position of the first sidelobe. The time reference of the pulse in the spectral profile is shifted toward the end of the pulse, hence leading to some self-refocusing in the spectral domain. This leads to a main lobe toward the end of the pulse, which reduces relaxation, flow, and motion effects.

To determine the SPSP pulse ρ, the following equation has to be inverted

$$A\rho = b. \qquad [6]$$

This was solved in a linear least-squares sense by computing

$$\rho = (A^{\top}A)^{-1}(A^{\top}b). \qquad [7]$$

Typical computation times are a few seconds on standard computers.

The pulse was designed to be a general purpose pulse for exciting and separating all five metabolites (Pyr, Ala, Pyr-Hydrate, Lac, BC), while maintaining a sufficiently large spectral passband against typical B_0 offsets. The most closely spaced resonances are Ala and Pyr-hydrate with 90 Hz shift difference on $B_0 = 3\,$T. Typical B_0 variations in the abdominal rat regions at 3 T on proton frequency (128 MHz) are up to 120 Hz, which translates to 30 Hz for ^{13}C spins due to the lower gyro-magnetic ratio. Therefore, a good compromise for the SPSP pulse design was a spectral bandwidth of 85 Hz and fractional transition width of FTW $= 0.7$. Sideband artifacts were chosen to fall into spectral areas with minimal contamination of other metabolites. The SPSP pulse is composed of 15 lobes each 1.12 ms long, has a total duration of 17.5 ms, and a minimum slice thickness of 8 mm ($f_0 = 32\,$MHz; $G_{\mathrm{max}} = 40\,$mT/m).

The complete 2D fitting approach helps to minimize sidelobe artifacts. The excitation profiles of the pulse simulated with the Bloch equations and measured in an NMR test tube filled with water doped with 2:100 parts of Dotarem is shown in Fig. 2.
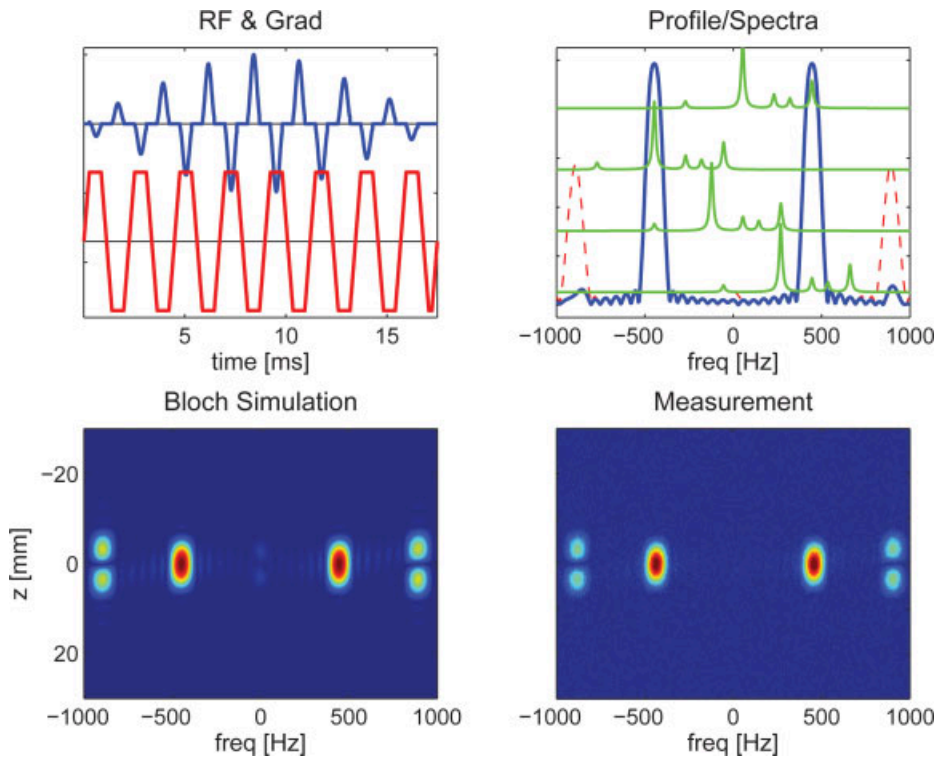
FIG. 2. SPSP excitation pulse and its profile. The pulse shape with radio-frequency and gradient modulation is shown on top left; the simulated and measured SPSP profiles in the bottom ($\theta = 90°$); and at the top right, the shifted spectra are plotted in green with the SPSP profile shown in blue (cross-section through slice center) and red (maximum). The four spectra in green are shifted to Lac, Pyr, BC, and Ala (from top to bottom, respectively). [Color figure can be viewed in the online issue, which is available at wileyonlinelibrary.com.]

Sequence and Reconstruction

For the final sequence, SPSP excitation is combined with a single-shot spiral readout trajectory, as shown in Fig. 3. Thus, one slice-selective image of one metabolite is acquired in a single excitation. The other metabolites are then excited by shifting the spectral frequency of the pulse according to the scheme depicted in Fig. 4. Hence, for imaging, the four metabolites Lac, Pyr, BC, and Ala

one needs four excitations (times the number of encoded slices). Besides the high encoding efficiency, the sequence also allows exciting the different metabolites with individual flip angles (Fig. 4). This typically means a lower flip angle θ_P for Pyr and larger ones for the downstream metabolites. In case of saturation-recovery, the other metabolites are excited and at the same time saturated with $\theta_X = 90°$.

The optimal selection of the parameters t_m and θ_X was simulated with the two-site exchange model (Eq. [1]) using the typical Pyr curve shown in Fig. 1. This curve is the average of curves measured slice-selectively through the rat heart, liver, and kidney using $\theta_P = 5°$. The input parameters for the simulation are k_{PX}, $T_{1,X,eff}$, θ_X, and t_m. The varying signal depletion of Pyr due to different k_{PX} and θ_P was neglected. For guiding the parameters selection, two different types of plots were made: one with the maximum SNR of X from a single acquisition, and one with the maximum SNR of X with the optimum number of acquisitions averaged. Simulations were performed for $k_{PX} = 0.01, 0.02, 0.03, 0.05\,s^{-1}$, $T_{1,X,eff} = 10, 20, 30\,s$, θ_X

FIG. 3. Pulse sequence used for metabolic-exchange rate imaging with saturation-recovery. After spectral and slice-selective excitation of a single metabolite, the image is encoded with a single-shot spiral readout. [Color figure can be viewed in the online issue, which is available at wileyonlinelibrary.com.]
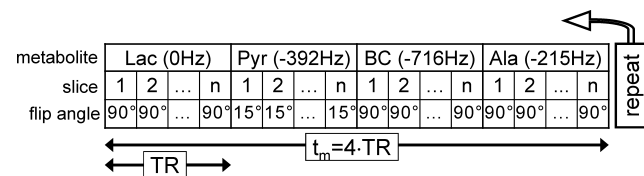
FIG. 4. Sketch of the used metabolite excitation scheme. Lac, Pyr, BC, and Ala are excited consecutively in the outer loop, while the different slices are iterated through the inner loop. Pyr is excited with a lower flip angle (15°), whereas the downstream metabolites are excited with 90° in case of saturation recovery.
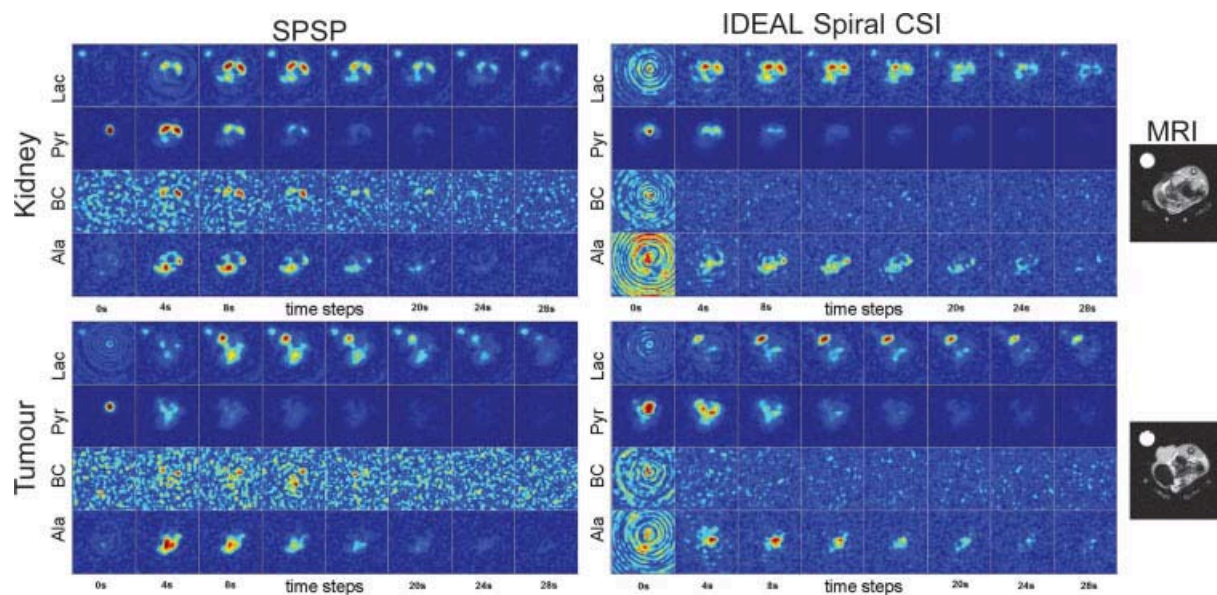
FIG. 5. In vivo metabolic images from rat grm02 062 through kidney (top) and tumor (bottom). SPSP and IDEAL Spiral CSI images are shown on the left and right, respectively. [Color figure can be viewed in the online issue, which is available at wileyonlinelibrary.com.]

values ranging from 0° to 90° in steps of 1°, and t_m values from 0.1 to 15 s in steps of 0.1 s.

The spiral trajectories were SNR optimized by matching the readout with the expected T_2^*. The spiral starts in the center of k-space at the beginning of the exponential free-induction decay, where the signal level is maximal. The highest spatial frequencies are encoded toward the end of the spiral readout. The readout duration is typically longer than T_2^* and the signal already disappeared into the noise. The reason for the long acquisition time is because it is desired to encode as much information as possible with the limited and nonrecoverable hyperpolarized signal. The SNR is optimized during the reconstruction by apodizing with a matched filter (33). T_2^* of ^{13}C spins is a quarter as compared to that of ^1H spins due to the lower gyromagnetic ratio of ^{13}C. Here, we assume $T_2^* = \frac{1}{\pi \cdot 15\,Hz} = 21.2$ ms as typical values in the rat body at $B_0 = 3$ T. Filtering the data with the matched Gaussian filter leads to a squared Gaussian signal decay, which results in an effective resolution of half the nominal resolution for a readout duration of 45 ms. The signal level remaining at the end of the readout is $\approx 0.2\%$ of the level at the start of the free-induction delay. Hence, the field of view is chosen such that with given maximum gradient strength and slew rate, the resulting spiral readout duration is 45 ms.

The acquired spiral data is reconstructed by various preprocessing steps, gridding onto a Cartesian grid (34) and finally a fast Fourier transformation. The preprocessing starts with a compensation for the gradient to radio frequency delay, an off-isocenter modulation to shift the images (according to the scan prescription), a bandpass filter, and finally, an apodization with a Gaussian filter with $lb = 15$ Hz. For the metabolic turnover images, the ratio between Lac and Pyr was computed and compensated for flip angles and t_m according to Eq. [3]. The regularization factor α was set to 20% of the maximum of the pyruvate signal through the slice.

Experimental

The SPSP pulses were implemented into a pulse-and-acquire sequence (FIDCSI) on a 3T GE parallel-transmit-modified HDx scanner (GE Healthcare, Milwaukee, WI). The spiral trajectories were stored in a file and read into the sequence. A dual-tuned ^{13}C-^1H rat-sized birdcage volume-resonator was used for radio frequency transmission and reception (35).

[1-^{13}C] Pyruvic acid doped with 15 mM Trityl OX063 radical and 1 mM Dotarem was polarized in a HyperSense DNP polarizer (OxfordInstruments, Abingdon, UK). After 1–2 h, it was rapidly dissolved by flushing with a hot aqueous solution containing 80 mM Trizma buffer, 80 mM NaOH, and 0.1 g/L Na-EDTA, leading to an 80 mM Pyr solution with physiological pH, osmolarity, temperature, and a liquid-state polarization of $\approx 25\%$. This solution (2.5 ml/kg) was injected into the tail vein of the rats (average weight ≈ 150 g), which were anesthetized with 1–3% Isoflurane. The animals were monitored for ECG, breathing, and temperature, and kept warm on a heating pad with circulating warm water. In total, four female Fischer 344 rats (Charles River, Sulzfeld, Germany) bearing subcutaneous Mat B III tumors were imaged. The animal study was approved by the local governmental committee for animal protection and welfare (Tierschutzbehörde, Regierung von Oberbayern).

Each rat received two injections within one examination using two different acquisition schemes for comparison. The time difference between the two injections was approximately 1 h. In both cases, four slices with 10 mm thickness were acquired in axial orientation including kidney and tumor. SPSP excitation using saturation recovery was acquired during the first injection using the following acquisition parameters: $t_m = 4$ s, $\theta_P = 15°$, $\theta_X = 90°$, excitation frequencies centered on Lac, Pyr, BC, and Ala, using the scheme shown in Fig. 4. For comparison, IDEAL

FIG. 6. Pyr, Lac, and turnover (k_{PL}) images of all four measured rats of the fourth time step. The colormap for k_{PL} is scaled to $0.08\,s^{-1}$, whereas the Pyr and Lac images are in arbitrary units. The tumors are highlighted by white arrows.
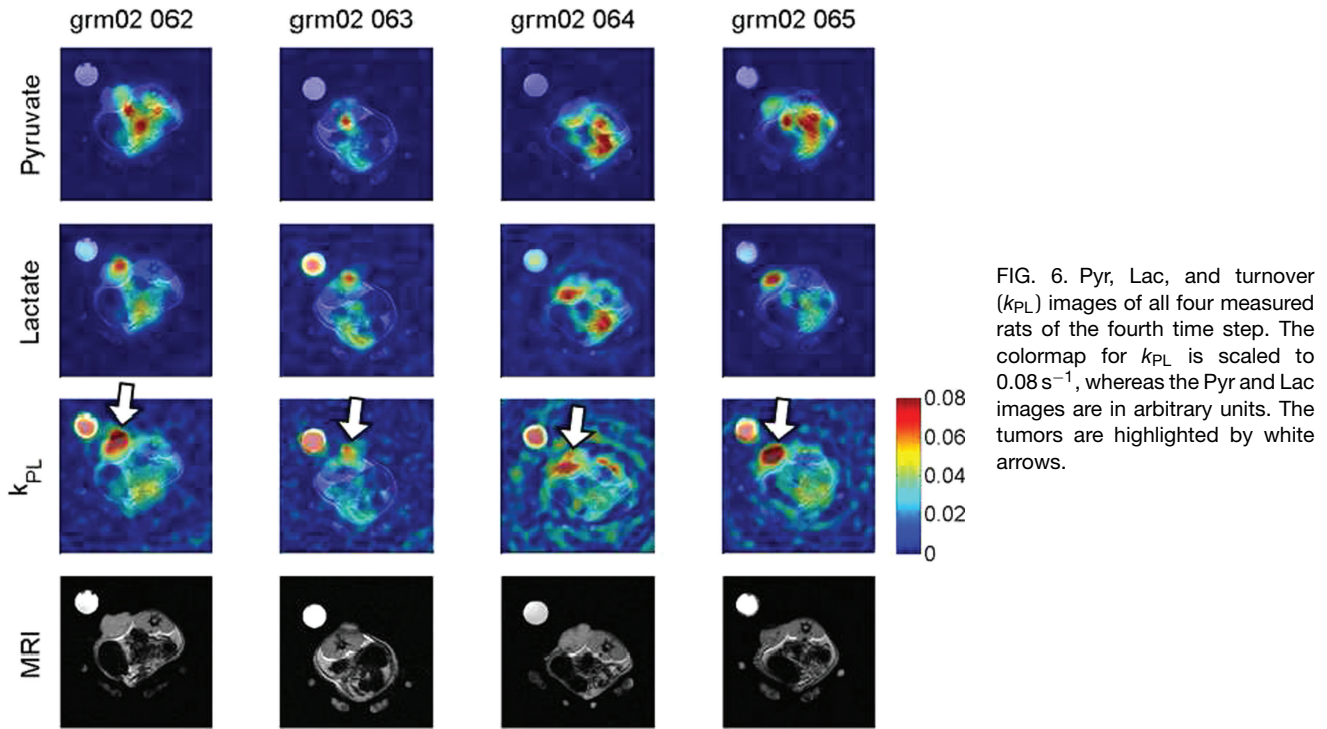
Spiral CSI (14) was acquired during the second injection sampling, the spectrum with seven shifted echoes, an echo time spacing of $1.12\,ms$, a flip angle $\theta = 10°$ and a sequence pulse repetition time of $500\,ms$, leading again to the same temporal resolution of $4\,s$. Both measurements used the same spiral trajectory with field of view of $80\,mm$, maximum gradient strength of $22\,mT/m$, and slewrate of $73\,mT/m/ms$, a trajectory duration of $45\,ms$, and 32×32 nominal matrix size. With an assumed in vivo linewidth on ^{13}C frequency of $15\,Hz$ and a matched filter of another $15\,Hz$, this leads to a real matrix size of 16×16, equivalent to $5 \times 5\,mm^2$ pixel size.

FIG. 7. Metabolite SNR averaged over the four rats (mean $\pm$ standard deviation) for SPSP (blue dashed line) and IDEAL (red solid line).
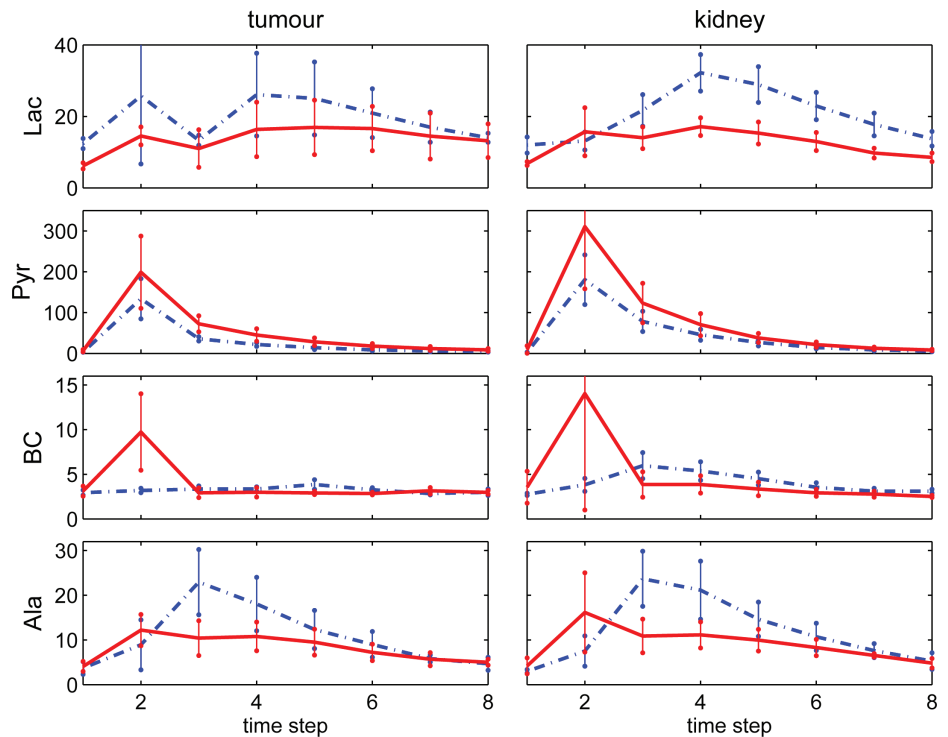
RESULTS AND DISCUSSION

The SNR simulations with Eq. [1] of SPSP excitation with respect to flip angle θ_X and metabolite repetition time t_m are shown in Fig. 8 for $T_{1,X,\text{eff}} = 20\,\text{s}$ and $k_{PX} = 0.02\,\text{s}^{-1}$. Although the absolute signal level is varying significantly for the simulations with the different k_{PX} and $T_{1,X,\text{eff}}$ values, the qualitative behavior of the curves remains the same (data not shown). When looking at the averaged SNR, one can see a continuous line with constant maximal signal level. For $t_m = 1, 2,$ or $4\,\text{s}$, one would choose for instance $\theta_X \approx 20, 30,$ or $40°$, respectively. If one wants to optimize the SNR of a single time step, one would generally choose longer t_m in combination with a higher θ_P. In this work, $\theta_P = 90°$ and $t_m = 4\,\text{s}$ was chosen to demonstrate the saturation-recovery approach, while still retaining sufficient SNR.

Metabolite and turnover maps are shown in Figs. 5 and 6, respectively. Both are generally of good quality, SNR and reproducibility. The metabolite images of Lac, Pyr, BC, and Ala are compared between IDEAL Spiral CSI and SPSP in Fig. 5 for one representative rat (grm02 062) for a slice through the kidney and a slice through the tumor. SNR was calculated by dividing the maximum intensity through the standard deviation of the (complex) noise of the respective metabolite images. The SNR of the downstream metabolites is generally better with SPSP as compared to IDEAL, as shown in Fig. 7. Averaging the ratio of SNR of SPSP over IDEAL over the four rats and over time steps two to six shows an increase in Lac SNR by a factor of 1.5 ± 0.31 and 1.61 ± 0.13 in tumor and kidney, respectively. Pyr shows a decrease in SNR by a factor of 0.6 ± 0.38 and 0.67 ± 0.04, whereas Ala shows an increase in SNR by a factor of 1.45 ± 0.14 and 1.49 ± 0.15 for the slice through the tumor and kidney, respectively. BC is generally not detectable with IDEAL but sometimes visible with SPSP in the kidneys. Ala is generally not present in this tumor model but often high in the abdomen of the rats.

IDEAL shows a spiral blurring artifact in the first time step (right column in Fig. 5), which can stem from high Pyr level and transient signal dynamics. A too high Pyr level in the blood vessel cannot be sufficiently resolved with the seven echo times and is bleeding into the other metabolites as off-resonance rings. Furthermore, the metabolites show a high dynamic change during the acquisitions of the seven echoes of the first time step, which might also induce this blurring artifact. This artifact is significantly reduced for SPSP, hence showing the good spectral selectivity of the applied pulses. SPSP has the advantage of acquiring and encoding the whole slice in a single shot, which leads to more consistent data and reduced sensitivity to flow, motion, or transient signal dynamics.

Metabolic-exchange rate images for Lac of all four rats are shown in Fig. 6 for the fourth time step. All four tumours show an elevated lactate turnover k_{PL}, clearly separating the tumors from the other tissue. This is in contrast to the pure Lac images, where signal is often visible in the abdomen as well. However, Pyr is increased there as well, indicating that there is no increased metabolic exchange activity present. The Pyr and Lac images (top and middle in Fig. 6) are scaled to the maximum signal, i.e., plotted in arbitrary units, because of the inherent difficulty of absolute quantification in MR, particularly hyperpolarized MR.
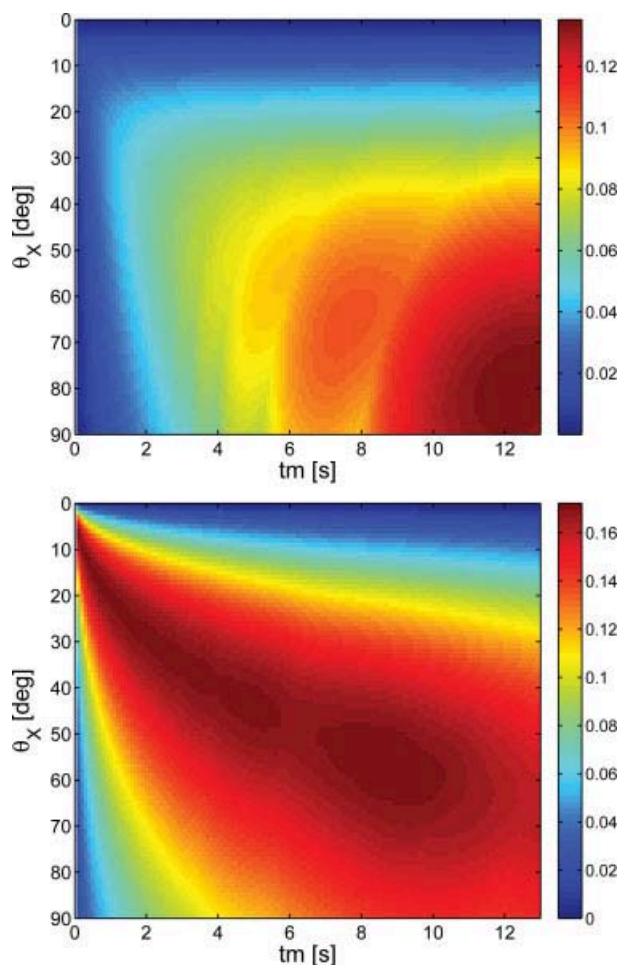
FIG. 8. Signal levels using two-site exchange model simulations as shown in Fig. 1, with a varying flip angle θ_X and metabolite repetition time t_m. The plot on top shows the maximum signal of the time curve. The plot below shows the averaged signal level, attained by averaging the SNR-optimal number of points. Simulations shown here use $T_{1,X,\text{eff}} = 20\,\text{s}$ and $k_{PX} = 0.02\,\text{s}^{-1}$. [Color figure can be viewed in the online issue, which is available at wileyonlinelibrary.com.]

The exchange rate images (bottom in Fig. 6) are scaled to $k_{PL} = 0.08\,\text{s}^{-1}$, which represent physiologically realistic values (6). This demonstrates the quantitative nature of the proposed method. Note that some of the tumors were already necrotic, while some were still fairly small. Elevated exchange rates were always detected despite the different stages of the tumors.

CONCLUSIONS

A method for metabolic turnover mapping based on a selective saturation of downstream metabolites and their subsequent recovery due to metabolic conversion from Pyr was introduced in this work. This is a first step toward a more quantitative metabolic imaging approach, as the images of metabolite levels are usually in arbitrary units. Several improvements for SPSP pulse design and the spiral readout were presented and demonstrated.